ACS OMEGA

http://pubs.acs.org/journal/acsodf

Article

Study on Gas Explosion Propagation Law and Explosion Venting in an Excavation Roadway

Ke Gao,* Zemiao Yang, Shuai Yang, and Shengnan Li

Cite This: *ACS Omega* 2023, 8, 5257−5273

Read Online

ACCESS | Metrics & More | Article Recommendations

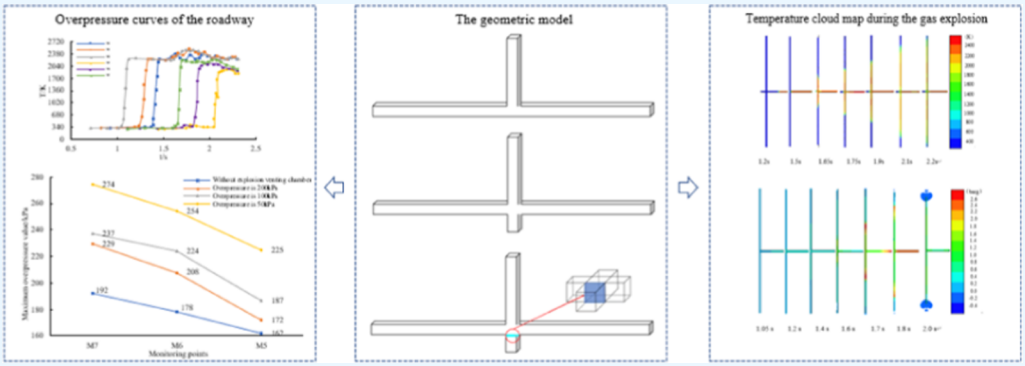

ABSTRACT: Gas explosions are the biggest threat to coal mine safety, which often result in sudden massive destruction. When a gas explosion occurs in a mine, it often causes a large number of casualties and property losses, which significantly restricts the development of the coal industry. In this study, a numerical model was established for the excavation and main roadways under the condition of a forward blasting chamber and a blasting wall, and the law of overpressure propagation and the flame temperature were studied. The results show that the overpressure curve first increases and then decreases with time, exhibiting a fluctuating state, and finally tends to stabilize. The overpressure curve with an explosion venting chamber and explosion venting wall oscillates many times; compared with the roadway overpressure reduced by 10% and explosive impulse reduced by 8.5%, the explosion venting chamber and explosion venting wall have a certain explosion venting effect. The flame temperature exhibits a gradual increase in the early stage, a sharp increase in the temperature at the measuring point, a fluctuation in the temperature curve in the later stage, and a significant decrease after the roadway turns. The explosion venting chamber and explosion venting wall with different explosion venting pressures have a slight effect on the temperature of each measuring point in the roadway after a gas explosion.

INTRODUCTION

China is among a few countries that regard coal as a key resource.[1] Additionally, China's coal production ranks first in the world; it accounts for more than half of the world's total coal production, and the strategic position of China's coal resources will continue for a long time.[2] Coal is not only an important power fuel but also an important industrial raw material.[3] Therefore, the safety of coal production has become a priority. According to relevant statistics, in the 13 years from 2008 to 2020, 1085 accidents occurred in coal mines in China (Hong Kong, Macao, and Taiwan are not included), of which 926 fatal accidents occurred and 4493 people died.[4,5] Of these, most (33%) deaths occurred due to gas accidents;[6] gas accidents occur most frequently, accounting for about 70%. For a long time, coal and gas outbursts have posed a significant threat to the safe and efficient function of coal mines.[7] As one of the five traditional natural disasters in coal mines, when a gas explosion accident occurs, the consequences are extremely severe. As the most likely location of gas emission occurs underground, the study of gas explosion characteristics and explosion venting measures is the focus of coal mine safety production.[8−12]

Scholars worldwide have conducted theoretical analyses,[13] numerical simulations,[14−16] and experimental tests;[17,18] other means of gas explosion mechanism characteristics, propagation law, and the status of explosion venting research are also deepening. Dorofeev[19] briefly introduced the acceleration of flames and applied the flame acceleration mechanism to the explosion process. Lee[20] described the acceleration of flames and the process of deflagration to detonation in detail for the

Received: September 4, 2022
Accepted: January 5, 2023
Published: January 30, 2023

https://doi.org/10.1021/acsomega.2c05740
ACS Omega 2023, 8, 5257−5273

first time. Ciccarelli[21] systematically discussed the research results of the deflagration-to-detonation transition (DDT) process. To gain a deeper understanding of flame acceleration and ultimately detonation, Oran[22] applied the method of numerical simulation to this research. Baoshan et al.[23] used CHEMKIN-III software to analyze the chemical reaction mechanism of gas explosions using a sensitivity analysis program block, and they observed that the reaction steps had a significant influence on the reaction kinetics characteristics of the gas explosion process. Berthelot and Vieille[24] studied the detonation of flame propagation. Kangan[25] studied DDT in the process of gas explosion flame propagation under certain pipeline conditions. Fairweather[26,27] conducted gas explosion experiments in semi-closed pipes and observed that in the early stage of the explosion, the flame propagated along the wall of the pipe in a laminar state, and in the later stage of the explosion, the propagation speed accelerated and became a turbulent state, and the explosion pressure increased significantly. Lebecki[28] studied the transformation of a pressure wave into a shock wave during an explosion. Sa Wenke[29] performed the gas explosion experiment in the pipeline with the change in the cross section and direction and studied the change in the shock wave propagation law. Wenke studied the propagation of shock waves when bifurcation and turning occurred in an experimental pipeline and obtained the attenuation law of shock waves. Jinzhang and Tao[30] established a prediction model for the relationship between the gas explosion shock wave overpressure in the excavation roadway, gas concentration, propagation distance, and volume of the methane−air mixture. Wagner[31] and Moen[32] observed that the propagation speed of gas explosion flame in the pipeline with obstacles is 24 times that without obstacles, and the explosion pressure increases abruptly in the presence of obstacles. Alexiou et al.[33] designed a cylindrical container with a length−diameter ratio of 15.4 and filled with a 10% gas−air mixture. The effect of the explosion venting position on explosion venting was studied experimentally. They observed that the closer the ignition position was to the explosion venting outlet, the smaller the maximum shock wave overpressure. Cybulskii[34−42] and others studied various types of explosions and explosion-suppression methods through many numerical simulations and experiments. They observed that the explosion-suppression effect is affected by various factors such as material type, spatial distribution, and explosion-suppression space. Juncheng et al.[43] and Wei et al.[44] used a large and small spherical explosion vessel and pipe to form a connector to discharge the process of a closed explosion. Combined with experiment and numerical simulation, the propagation law of flow field, flame, and pressure under different explosion venting conditions was studied and analyzed.

Based on the abovementioned research review, only a few studies have been conducted on the gas explosion propagation law and explosion relief in the forward blasting chambers of excavation roadways. Water barriers are generally used nowadays in coal mines. New suppression techniques were also investigated such as vacuum chamber, SiO2 fine powders, ABC powder, water mist, and others. However, the overpressure cannot be suppressed by the techniques which will lead to serious accidents. In this study, the venting of the forward venting chamber in excavation roadways was studied to obtain the relevant explosion characteristics and laws and reduce the damage of explosion to roadways. The results are useful for the safe production of coal mines, providing support for gas disaster control and preventing the occurrence of gas explosion accidents in coal mines.

1. NUMERICAL SIMULATION PRINCIPLE OF GAS EXPLOSION

1.1. General Equations. Gas explosion is a rapid combustion reaction process, which satisfies the mass, momentum, and energy conservation and chemical composition equilibrium equations. The basic equations are decomposed and averaged by Reynolds. Under the condition of isotropic turbulence, the concept of the isotropic turbulence viscosity coefficient is introduced, and the following time-averaged equations of homogeneous turbulent combustion can be obtained.

Mass conservation equation

$$\frac{\partial \rho}{\partial t} + \frac{\partial}{\partial x_i}(\rho u_i) = 0 \tag{1}$$

Momentum equation

$$\frac{\partial}{\partial t}(\rho u_i) + \frac{\partial}{\partial x_i}\left(\rho u_j u_i - \mu_{\text{eff}}\frac{\partial u_i}{\partial x_j}\right) = \frac{\partial p}{\partial x_i} + \frac{\partial}{\partial x_j}\left(\mu_{\text{eff}}\frac{\partial u_j}{\partial x_i}\right) - \frac{2}{3}\frac{\partial}{\partial x_j}\left[\delta_{ij}\left(\rho k + \mu_{\text{eff}}\frac{\partial u_k}{\partial x_k}\right)\right] \tag{2}$$

Energy equation

$$\frac{\partial}{\partial t}(\rho h) + \frac{\partial}{\partial x_j}\left(\rho u_j h - \frac{\mu_{\text{eff}}}{\sigma_h}\frac{\partial h}{\partial x_j}\right) = \frac{Dp}{Dt} + S_h + S_{h,\text{rad}} \tag{3}$$

Chemical composition equilibrium equation

$$\frac{\partial}{\partial t}(\rho Y_{\text{fu}}) + \frac{\partial}{\partial x_j}\left(\rho u_j Y_{\text{fu}} - \frac{\mu_{\text{eff}}}{\sigma_{\text{fu}}}\frac{\partial Y_{\text{fu}}}{\partial x_j}\right) = R_{\text{fu}} \tag{4}$$

where x and $t$are spatial and temporal coordinates, respectively; ρ, p, h, and Y_{fu} are the density, pressure, total enthalpy, and combustible gas mass fraction, respectively; k is the turbulent kinetic energy; u_i is the velocity component in the i direction; subscripts i, j, and k are summation conventions; μ_{eff} is the effective viscosity; R_{fu} is the time-averaged combustion rate of the gas mixture; and σ is the Prandtl number.

$S_h = T_{ij}\frac{\partial u_i}{\partial x_j}$ and $T_{ij} = \mu_{\text{eff}}\left(\frac{\partial u_i}{\partial x_j} + \frac{\partial u_j}{\partial x_i}\right) - \frac{2}{3}\mu_{\text{eff}}\frac{\partial u_k}{\partial x_k}$; $S_{h,rad}$ is the original term of radiation due to coupled radiation, defined in the radiation model. $\mu_{\text{eff}} = \mu_l + \mu_t$, μ_l is the molecular viscosity, $\mu_t = \frac{C_\mu \rho k^2}{\varepsilon}$, C_μ is the empirical constant, and δ_{ij} is the Kronecker symbol, $\delta_{ij} = \begin{cases} 1 & i = j \\ 0 & i \neq j \end{cases}$.

1.2. Combustion Model. Ignition of a fuel and oxidizer premix cloud may escalate to an explosion. The fuel and oxidant stabilized non-turbulent premix will burn at laminar combustion rates before escalating to an explosion.

$$S_L^0 = S_L^0\,(\text{fuel}, \Phi) \tag{5}$$

where Φ is the equivalence ratio and the laminar combustion rate depends on the fuel and the equivalence ratio Φ. For mixtures with fuel content below the lower flammable limit or

https://doi.org/10.1021/acsomega.2c05740
ACS Omega 2023, 8, 5257−5273

above the upper flammable limit, the laminar combustion rate is equal to zero, that is, it does not burn. In an explosion, the flame accelerates and becomes a turbulent flame. Turbulent combustion velocity is much greater than laminar combustion velocity due to better mixing of reactants and products.

The reaction area in the premixed flame is sparse compared to the actual grid resolution. In the simulation, the flame area is made denser by increasing the diffusion by a β-factor and decreasing the reaction rate by a $1/\beta$-factor. Therefore, the flame model in this paper is called the β-flame model.

Fuel transport equation

$$E = \frac{\mu_{\text{eff}}}{\sigma_{\text{fuel}}} \tag{6}$$

where E is the diffusion coefficient of the fuel; in addition, a dimensionless reaction rate W can be defined. In the β−flame model, E and W are adjusted as follows.

$$W' = \frac{W}{\beta} = W\frac{l_{LT}}{\Delta g} \tag{7}$$

$$E' = E\beta = E\frac{\Delta g}{l_{LT}} \tag{8}$$

Based on the eigenvalue analysis of the combustion rate, the following relationship between the diffusion coefficient E and the dimensionless reaction rate W was obtained for the progress variable x_q = 0.05.

$$WE = 1.37S_u^2 = W'E' \tag{9}$$

W' and E' depend on the grid size and the burning rate, and the equations are as follows

$$E' = C_{1\beta}S_u\Delta gE\beta \tag{10}$$

$$W' = C_{1\beta}\frac{S_u}{\Delta g} \tag{11}$$

The reaction rate expression for the fuel is as follows

$$R_{\text{fu}} = -W'\rho \min[\delta_H(x - x_q), \quad x, 9 - 9x] \tag{12}$$

where δ_H is the Heaviside step function.

1.3. Equation Discretization and Solution Method. The numerical simulation uses a standard turbulence model, the geometry is represented by the idea of the distributed porous structure, and the flame smaller than the grid scale is represented by a sublattice model. In the process of numerical modeling, the turbulent time-averaged system of equations is chosen to describe the flow field, the k-ε turbulence model is used to describe the turbulence variation during the combustion process, the β-flame model is used to describe the variation of the combustion reaction rate during the combustion process, and the wall function method is used to deal with the variation of the flow field in the near-wall region.

The discrete equations are derived using the control volume method integral method with a staggered grid technique, a central difference format for the diffusion term, a local linearization method for the source term, and the SIMPLE algorithm for the pressure−velocity coupling problem. The finite volume method is used to solve the compressible N−S equation under three-dimensional Cartesian grid conditions. The alternating direction iterative method is used to solve the algebraic system of equations (inner iteration), and the nonlinear relations are handled by iteration in a sub-relaxation manner (outer iteration).

2. NUMERICAL SIMULATION OF GAS EXPLOSION PROPAGATION CORRESPONDING TO THE EXPERIMENT

2.1. Model Establishment and Boundary Condition Setting. An excavation roadway with a size of 100 m × 4 m ×

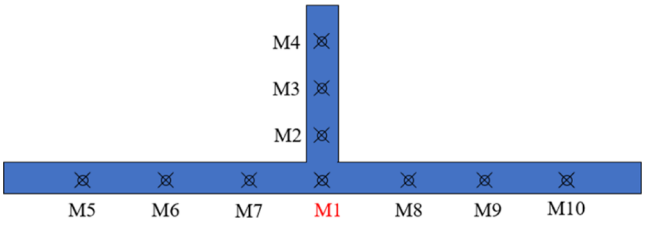

Figure 1. Distribution map of monitoring points.

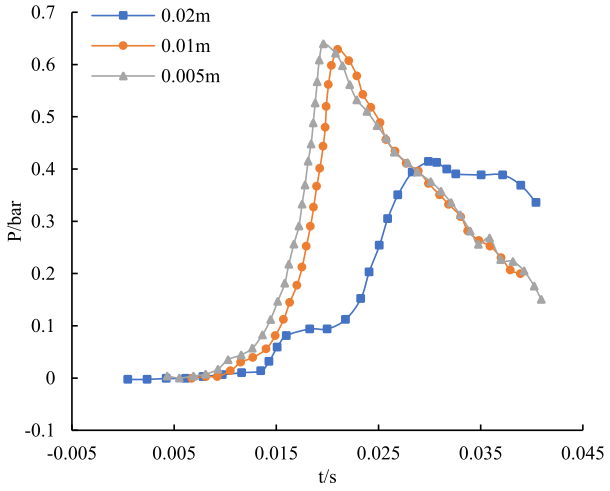

Figure 2. Explosion pressure−time curves for different grid sizes.

3 m and a roadway with a size of 400 m × 4 m × 3 m were established. The two ends of the roadway were opened, and the two were combined to form an inverted T-connected geometric model. The entire model had 10 monitoring points. Measuring point M1 was at the intersection of the excavation roadway and the main roadway and was used as a reference. M2, M3, and M4 were in the excavation roadway and were 25, 50, and 75 m away from M1, respectively. M7, M6, and M5 were in the left lane at 50, 100, and 150 m away from M1, respectively.

The model and location of monitoring points in the model are shown in Figure 1.

The initial conditions were set as follows: the mixture gas was in a normal temperature and pressure state before ignition. Assuming that the initial time is t_0, the initial conditions were $T(t_0) = T_0 = 20$ °C and $P(t_0) = P_0 = 100{,}000$ Pa; the gas was filled in the entire excavation roadway; and the gas concentration was 10%. Ignition was performed using point explosion, and the ignition point was set at the center of the tunneling head. It was an "Euler" boundary condition. The velocity along the roadway wall was $u = v = w = 0$, and the normal pressure, temperature, and density were set to 0.

A numerical simulation of the gas explosion process without a venting chamber was performed, in which the gas was filled

https://doi.org/10.1021/acsomega.2c05740
ACS Omega 2023, 8, 5257−5273

Table 1. Shock Wave Overpressure (bar)

monitoring points	1	2	3	4	5	6	7	8
location of the monitoring point (L/D)	20	23	50	51	54	68	54	68
measured value	0.652	0.678	0.764	0.986	0.662	0.556	0.662	0.556
simulation value	0.778	0.785	0.921	1.071	0.759	0.632	0.759	0.632

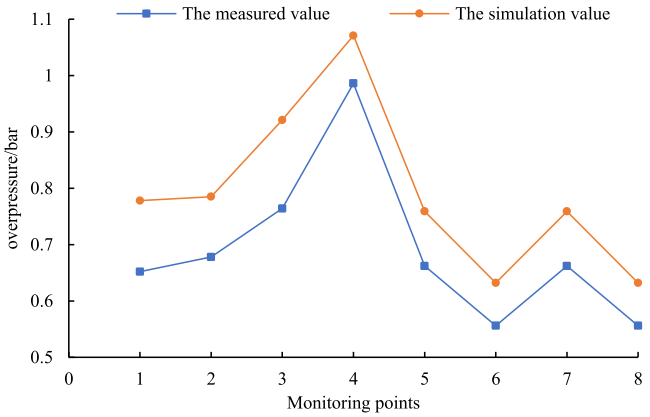

Figure 3. Comparison of experimental and simulation overpressures.

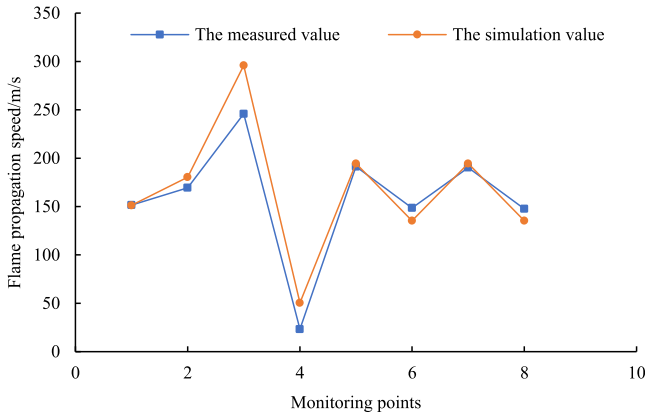

Figure 4. Comparison of experimental and simulated flame propagation speeds.

in the excavation roadway. Because the model was symmetric, the simulation results of M5, M6, and M7 were the same as those of M10, M9, and M8, respectively; therefore, the simulation results of M10, M9, and M8 are not analyzed in this paper.

2.2. Meshing and Grid Independence Verification. The abovementioned model was evenly meshed, and the mesh sizes were selected as 0.02, 0.01, and 0.005 m. Figure 2 shows the change curve of gas explosion pressure with time at the same monitoring point in the model under different grid sizes. As the figure shows, the trend of the gas explosion pressure−time curve when the grid size was 0.01 m was generally consistent with that when the grid size was 0.005 m, and the difference between them was not significant. Too sparse a meshwork would result in a large error in the simulation, and the actual results cannot be obtained. If it is too dense, the number of calculations is excessively large and the calculation would require a long time. Therefore, in this study, the grid size was selected as 0.01 m and the time step was 0.0025 s.

2.3. Comparison of Simulation and Experimental Results. *2.3.1. Comparative Analysis of Overpressure Data.* Table 1 shows the experimental and simulated values of the overpressure of the shock wave at each measuring point when the gas explosion propagated in the inverted T-shaped pipeline, where the experimental value was the arithmetic average of multiple measured data.

According to Table 1, the experimental and simulated overpressure curves of the shock wave were obtained at eight measuring points when the gas explosion propagated in an inverted T-shaped pipeline. Figure 3 shows that in pipeline T1, the overpressure value of the gas explosion shock wave increased with the increase in the propagation distance, but the increase was small. At the end of pipeline T1, the peak overpressure value of the shock wave reached the maximum. After entering pipelines T2 and T3, the peak overpressure of the shock wave increased first and then decreased rapidly.

2.3.2. Comparative Analysis of Flame Propagation Velocity Data. Table 2 shows the experimental and simulated values of the flame propagation velocity at each measuring point when the gas explosion propagated in the inverted T-shaped pipeline, where the experimental value was the arithmetic average of multiple measured data.

According to Table 2, the experimental and simulated propagation velocity curves were obtained at eight measuring points of the flame when a gas explosion propagated in an inverted T-shaped pipeline (Figure 4). Figure 4 shows that before the end of T1, the flame propagation velocity of the gas explosion increased, but the increase was small. In the last section of T1, the flame propagation velocity decreased sharply and almost approached zero, and then, the flame propagated to sections T2 and T3. When the flame entered T2 and T3, the propagation velocity initially increased and then decreased.

2.3.3. Error Analysis. Table 3 lists the errors of the overpressure value of the gas explosion propagation wave and flame propagation velocity value between the experimentally measured and numerically simulated values in the inverted T-shaped pipeline. According to Table 3, the maximum error between the simulated overpressure value and the experimental overpressure value at monitoring point 3 was 20.5%, and the minimum error at monitoring point 4 was 8.6%. The maximum error between the simulated and experimental flame propagation velocities at monitoring point 3 was 16.9%, and the minimum error at monitoring point 1 was −0.13%.

Table 2. Flame Propagation Speed Values ($m \cdot s^{-1}$)

monitoring points	1	2	3	4	5	6	7	8
location of monitoring point (L/D)	20	23	50	51	54	68	54	68
measured value	151.5	169.4	245.9	23.3	191.3	148.6	190.3	147.6
simulation value	151.3	180.4	295.9	50.5	194.5	135.3	194.5	135.3

https://doi.org/10.1021/acsomega.2c05740
ACS Omega 2023, 8, 5257−5273

Table 3. Error Table of Simulated and Measured Values

monitoring points	1	2	3	4	5	6	7	8
overpressure error	19.3%	15.8%	20.5%	8.6%	14.7%	13.7%	14.7%	13.7%
flame propagation velocity error	−0.13%	6.5%	16.9%	16.7%	1.7%	−9.0%	2.2%	−8.3%

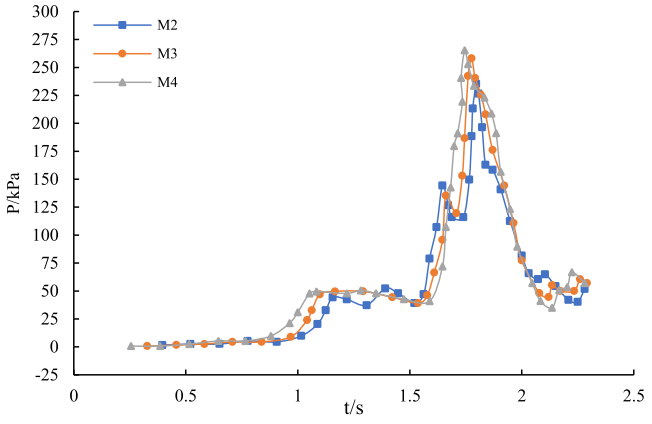

Figure 5. Variation law of overpressure at each monitoring point. (a) Change law of overpressure in measuring points in excavation roadways. (b) Change law of overpressure in measuring points in roadways.

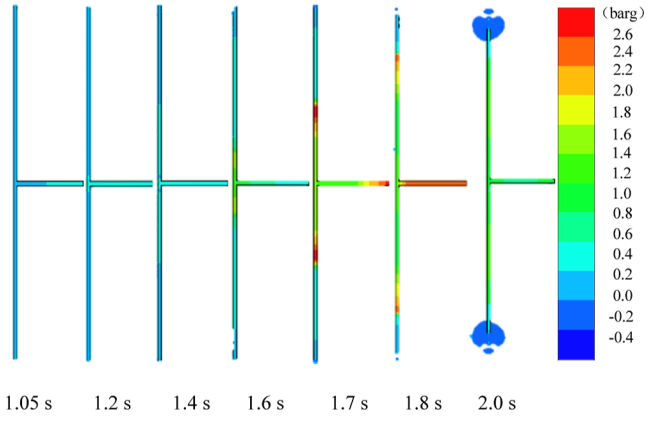

Figure 6. Pressure cloud diagram during gas explosion.

Figures 3 and 4 show that the numerical simulation results were larger than the experimental results because the heat exchange and roughness of the pipeline wall, as well as the quality of mixed gas and other factors, were not considered in the numerical simulation process, resulting in the large simulation results. In addition, the pipeline in the experiment could not be completely sealed and was connected with tee devices, which hindered the propagation of gas explosion and resulted in small experimental results. Although a deviation was observed between the numerical simulation and experimental results, the trend was the same. Thus, the model selected in this study can effectively reflect the propagation law of an actual gas explosion.

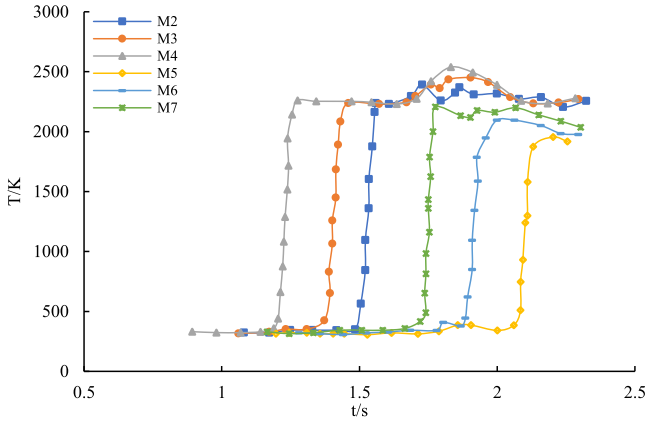

Figure 7. Temperature variation at various measuring points in the roadway.

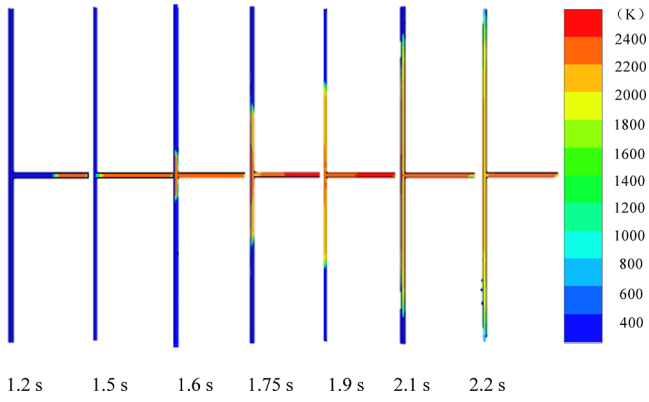

Figure 8. Temperature cloud map during the gas explosion.

2.4. Variation Law of Gas Explosion Overpressure in the Roadway. Figure 5 describes the variation in overpressure values of measuring points M2, M3, and M4 in the excavation roadway and the variation in overpressure values of M5, M6, and M7 in the main roadway with the explosion time. After gas explosion, the propagation evolution law of measuring point overpressure in the excavation roadway was the same, and the propagation evolution law of measuring point overpressure in the roadway was the same. Before 1.5 s in the initial stage of the explosion, it belonged to the deflagration stage, and the pressure gradually increased to a certain level. Figure 5b shows that the closer to the explosion source point, the shorter the

https://doi.org/10.1021/acsomega.2c05740
ACS Omega 2023, 8, 5257−5273

time for the overpressure to reach its peak value, and the farther away from the explosion source point, the longer the time for the overpressure to reach its peak value.

Figure 5 shows that the explosion overpressure of all monitoring points had multiple peaks. Owing to the reflection of the shock wave at the heading, wall of the roadway, and corner, the superposition of the reflected shock wave resulted in a phenomenon similar to the damping oscillation. As the reaction progressed, the explosion overpressure curve fluctuated several times and finally tended to be stable, which indicated that the explosion overpressure was not monotonically increasing and decreasing over time but fluctuating. When the explosion reaction was complete, the energy of the shock wave was gradually consumed owing to multiple reflections. After a period of propagation, the precursor wave no longer compressed the gas ahead and finally propagated at a stable speed. Here, the overpressure of each measuring point tended to be stable and remained unchanged.

As shown in Figure 6, we selected the dynamic pressure nephogram of gas explosion in the roadway at different times. The figure clearly shows the distribution law of gas explosion pressure at different times and positions in the roadway after the gas explosion. At the beginning of the explosion, the pressure gradually increased. At 1.2 s, the pressure wave reached the main roadway. At 1.4 s, owing to the expansion of the area at the corner, the mixed gas expanded, resulting in the expansion disturbance, weakening the shock wave intensity and distorting the wavefront. The airflow behind the wave moved around the corner to form a small vortex. At 1.7 s, the overpressure value of the heading head and middle part of the main roadway increased to the maximum. At 2.0 s, the pressure in the excavation and main roadways tended to be stable. Owing to the gas expansion and gas reflux at the outlet of the main roadway, a negative pressure zone appeared.

2.5. Variation Law of Gas Explosion Temperature in the Roadway. As shown in Figure 7, before the flame front reached each measuring point, because the gas was ignited, the flame propagation speed was low, and the temperature of each measuring point increased gradually at this time. When the flame front reached and passed through each measuring point, a large amount of combustion heat was released, and the temperature of each measuring point increased abruptly.

A comparison between different measuring points indicated that when the flame wave reached measuring points M4, M3, M2, M7, M6, and M5, the variation of flame temperature was basically the same, which increased abruptly and then tended to be stable. In addition, when the temperature reached the maximum, it was similar to the overpressure curve, and a fluctuation phenomenon occurred. This was because the flame wave entered the turning part, the combustion was uneven, and the flame was close to the exit, the heat diffused rapidly from the exit, and the reflux of the outlet airflow resulted in temperature fluctuations.

The maximum temperature values of measuring points M4, M3, M2, M7, M6, and M5 were 2544, 2482, 2400, 2223, 2112, and 1955 K, respectively. We observed that the farther away from the explosion source point, the smaller the maximum temperature value. After the flame turned into the main roadway, the temperature decreased significantly, and the maximum temperature at the explosion source point was 600 K higher than that near the outlet of the main roadway, indicating that the roadway turns hindered the propagation of the flame.

Figure 8 depicts the process of flame propagation using the change in temperature field in the combustion roadway. The temperature increased gradually from the explosion source point after the induction period of the gas explosion. At 1.5 s, the flame reached the corner of the roadway and began to propagate to both sides of the roadway, and the temperature was still in the increasing stage. At 1.75 and 1.9 s, in the corner of the roadway, the temperature was uneven, high, or low, which also indicated the late fluctuations of the temperature distribution curve. After 2.2 s, the flame spread to the exit of the roadway, and the flame temperature tended to be stable.

Before the flame front reached each measuring point because the gas was ignited, the flame began to spread gradually, and the temperature of each measuring point increased gradually at this time. When the flame front reached and passed through each measuring point, a large amount of combustion heat was released, and the temperature of each measuring point increased abruptly. In addition, the temperature curve fluctuated after the temperature increased abruptly. This was because the flame wave entered the turning part, the combustion was non-uniform, and the flame was close to the outlet; the heat diffuses rapidly from the outlet; and the effect of the backflow of the outlet airflow causes the temperature fluctuations.

3. NUMERICAL SIMULATION OF GAS EXPLOSION PROPAGATION IN THE EXPLOSION CHAMBER

3.1. Model Establishment and Boundary Condition Setting. The geometric model of the excavation and main

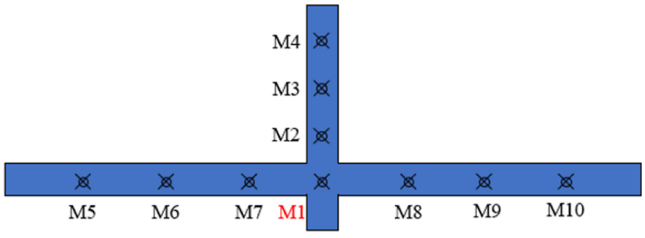

Figure 9. Model of the forward venting chamber for the excavation roadway.

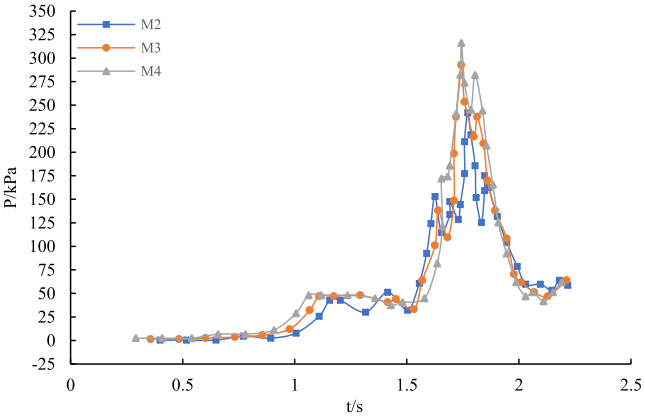

Figure 10. Change law of overpressure in measuring points in excavation roadways.

https://doi.org/10.1021/acsomega.2c05740
ACS Omega 2023, 8, 5257−5273

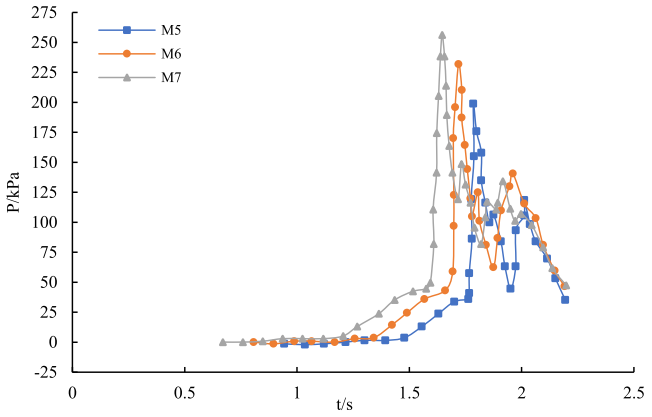

Figure 11. Change law of overpressure in measuring points in roadways.

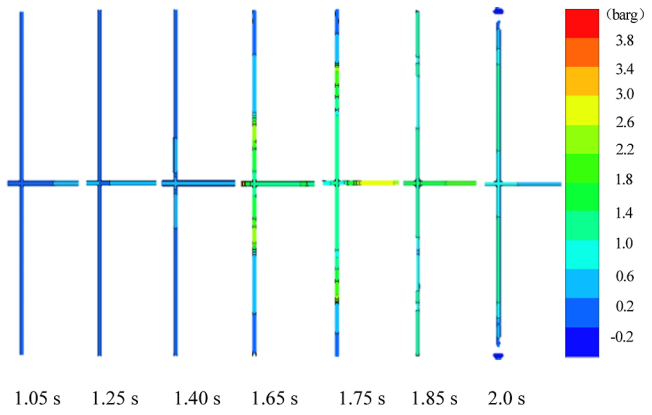

Figure 12. Pressure cloud diagram during gas explosion.

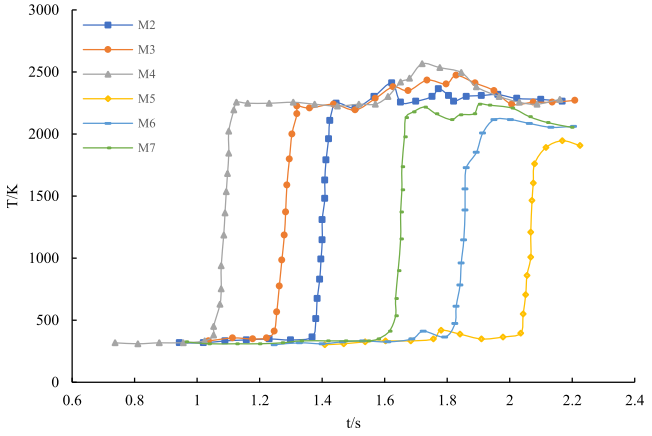

Figure 13. Temperature variation at various measuring points in the roadway.

roadways was consistent with the model of the non-explosive chamber, and the calculation area, grid division, and monitoring point setting of the whole model were the same as those of the non-explosive chamber. The difference was that an explosion venting chamber with a size of 5 m × 4 m × 3 m was added at the forward position of the tunnel. The specific model is shown in Figure 9.

The initial conditions were set as follows: the mixture gas was in a normal temperature and pressure state before ignition. Assuming that the initial time is t_0, the initial conditions were $T(t_0) = T_0 = 20$ °C and $P(t_0) = P_0 = 100{,}000$ Pa; the gas was

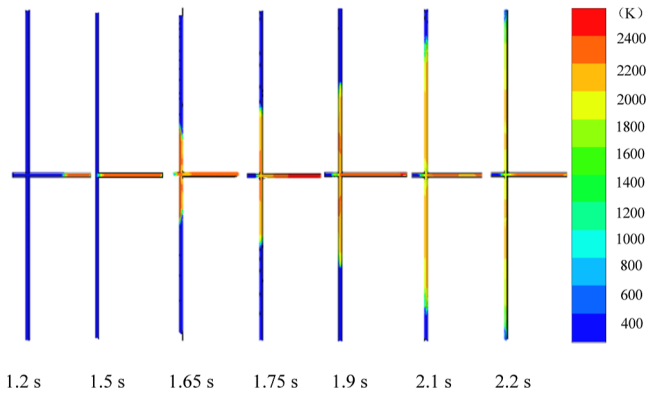

Figure 14. Temperature cloud map during gas explosion.

filled in the whole excavation roadway, gas concentration was 10%, and the ignition point was set at the heading head. The boundary condition was the Euler boundary condition. The velocity along the roadway wall was $u = v = w = 0$, and the normal pressure, temperature, and density were set to 0.

3.2. Variation Law of Gas Explosion Overpressure in the Roadway. Compared with the simulation without an explosion chamber, Figures 10 and 11 show that there were more peaks at each measuring point in the excavation and main roadways, that is, the number of shock wave oscillations increased. This was not only because the shock wave had reflections on the wall, driving head, and corner of the roadway but also because of the existence of the explosion venting chamber; after the shock wave reached the explosion venting chamber, the shock wave also reflected back and forth. This resulted in more complex shock wave reflections, resulting in more overpressure peaks. The overpressure curves of M2, M3, and M4 oscillated before the overpressure reached their maximum values, which was owing to the positive reflection of the shock wave in the explosion venting chamber. Most of the reflected shock waves in the explosion venting chamber had a positive reflection and reached the excavation roadway, resulting in more oscillations in the overpressure of M2, M3, and M4 in the excavation roadway.

Figure 12 shows the dynamic pressure cloud chart of gas explosion in the roadway at different times with the use of the explosion chamber. Figure 12 shows that the shock wave pressure began to increase at the initial stage of the gas explosion. At 1.25 s, the shock wave reached the explosion chamber for the first time, and the reflection caused the pressure at the exit of the roadway to decrease. At 1.40 s, a symmetrical low-pressure zone appeared at the corner of the roadway. After many reflections, at 1.65 s, the explosion chamber showed the highest pressure in the entire process, and the overpressure reached 400 kPa. The simulation results were consistent with the reflection theory of the shock wave described in Section 2 of Chapter 1. The simulation showed that the reflection of the shock wave strengthened the damage of the shock wave to the structure. At 2.0 s, when the pressure wave spread to the exit of the roadway, it stabilized.

3.3. Variation Law of Gas Explosion Temperature in the Roadway. Figure 13 shows that the variation law of the temperature curve was consistent with that without the explosion chamber. The temperature of each measuring point initially increased gradually, and when the flame reached the measuring point, the temperature increased abruptly to the maximum value and then fluctuated owing to uneven

https://doi.org/10.1021/acsomega.2c05740
ACS Omega 2023, 8, 5257−5273

combustion at the outlet and gas backflow. The farther away from the explosion source point, the smaller the maximum temperature value; the maximum temperature at the exit of the alley was significantly lower than the maximum temperature at the explosion source point. The maximum temperature values of measuring points M4, M3, M2, M7, M6, and M5 were 2573, 2486, 2410, 2243, 2147, and 1941 K, respectively.

The process of flame propagation is also explained by the change in temperature field in the combustion tunnel. Figure 14 shows that the flame reached the exit of the roadway at 1.5 s, and then, the flame did not directly enter the explosion chamber but first propagated to both sides of the roadway. This was because the shock wave reached the explosion chamber before the flame wave, and after many reflections, the pressure of the explosion chamber increased sharply. Therefore, the flame propagated to the area where the pressure was relatively small at the two ends of the roadway. At 1.65 s, the flame entered the explosion chamber, but we observed that the flame did not completely fill the explosion chamber in the entire process. After 2.2 s, the flame propagated to the exit of the two ends of the roadway, and the temperature was stable.

In the early stage of the explosion, the temperature initially increased gradually, and when the flame front passed the measuring point, the temperature increased abruptly, and then, the temperature curve exhibited a fluctuating state in the later stage owing to uneven combustion after turning and gas backflow at the outlet. After the flame turned into the main alley, the temperature decreased significantly, indicating that the turn of the roadway hindered the spread of the flame.

4. NUMERICAL SIMULATION OF GAS EXPLOSION PROPAGATION BY THE EXPLOSION DISCHARGE WALL

4.1. Model Establishment and Boundary Condition Setting. The geometric model of the excavation and main roadway was consistent with the model with the explosion venting chamber, and the calculation area, grid division, and setting of the monitoring points of the entire model were the same as those with the explosion venting chamber. The difference was that an explosion venting wall (the blue part in Figure 15) was added at the exit of the forward venting chamber of the tunnel. The specific model is shown in Figure 15.

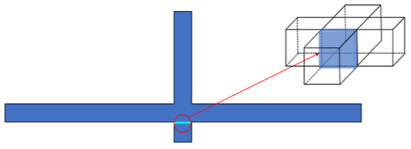

Figure 15. Schematic of the explosion venting wall.

The initial conditions were set as follows: the mixture gas was in a normal temperature and pressure state before ignition. Assuming that the initial time is t_0, the initial conditions were $T(t_0) = T_0 = 20$ °C and $P(t_0) = P_0 = 100{,}000$ Pa; the gas filled the whole excavation roadway, the gas concentration was 10%, and the ignition point was set at the heading head. The boundary condition was the Euler boundary condition. The velocity u along the roadway wall was $v = w = 0$, and the normal pressure, temperature, and density were set to 0.

4.2. Parameter Setting of the Explosion Discharge Wall. In the three-dimensional coordinate system, the vent wall is set to a rectangular plane; therefore, the one-dimensional is zero, which indicates the orientation of the plate. For example, if the dimension of the X direction is zero, the X direction is the normal direction of the plate. In this simulation, the dimension of the explosion-proof wall was set to zero in the X direction.

When the net pressure acting on the venting wall exceeds a given limit, the venting wall begins to yield, which we call the venting pressure (P_0). Therefore, two pressure values are given,

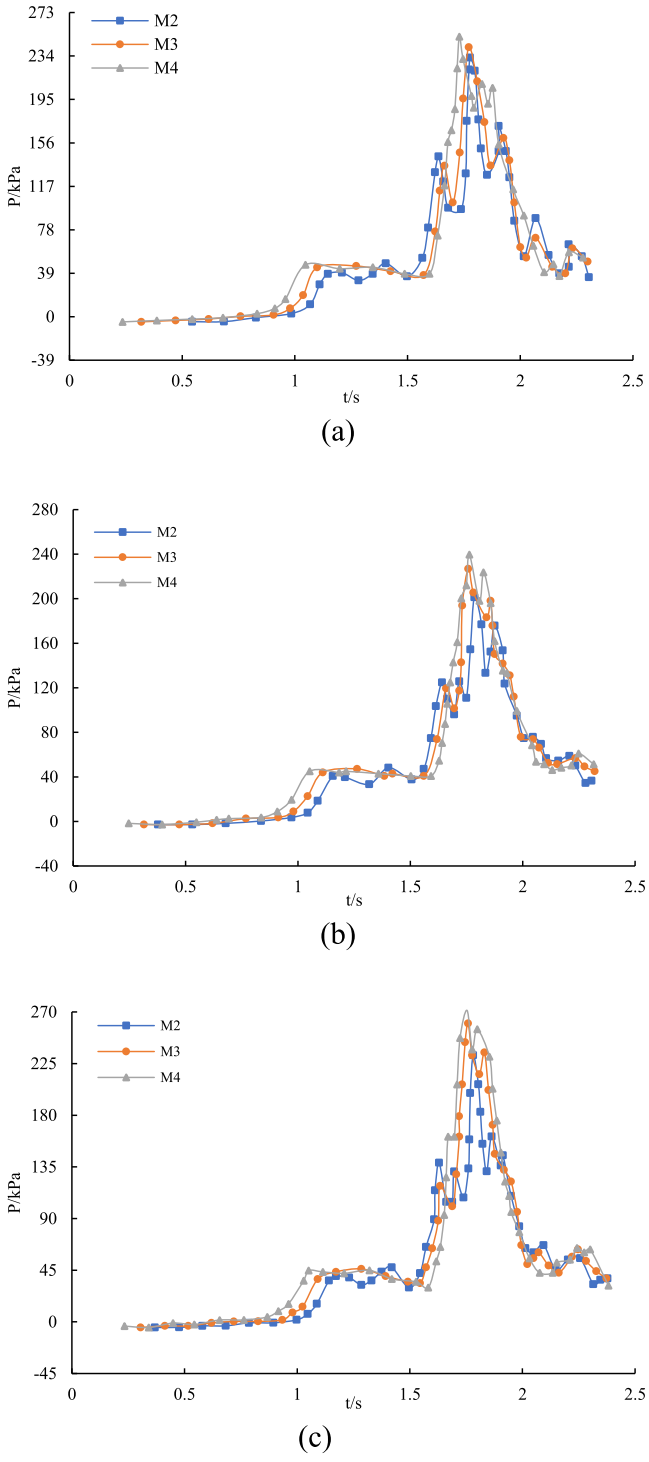

Figure 16. Overpressure curves of the excavation roadway under three explosion venting pressures. (a) Explosion pressure of 200 kPa. (b) Explosion pressure of 100 kPa. (c) Explosion pressure of 50 kPa.

https://doi.org/10.1021/acsomega.2c05740
ACS Omega 2023, 8, 5257−5273

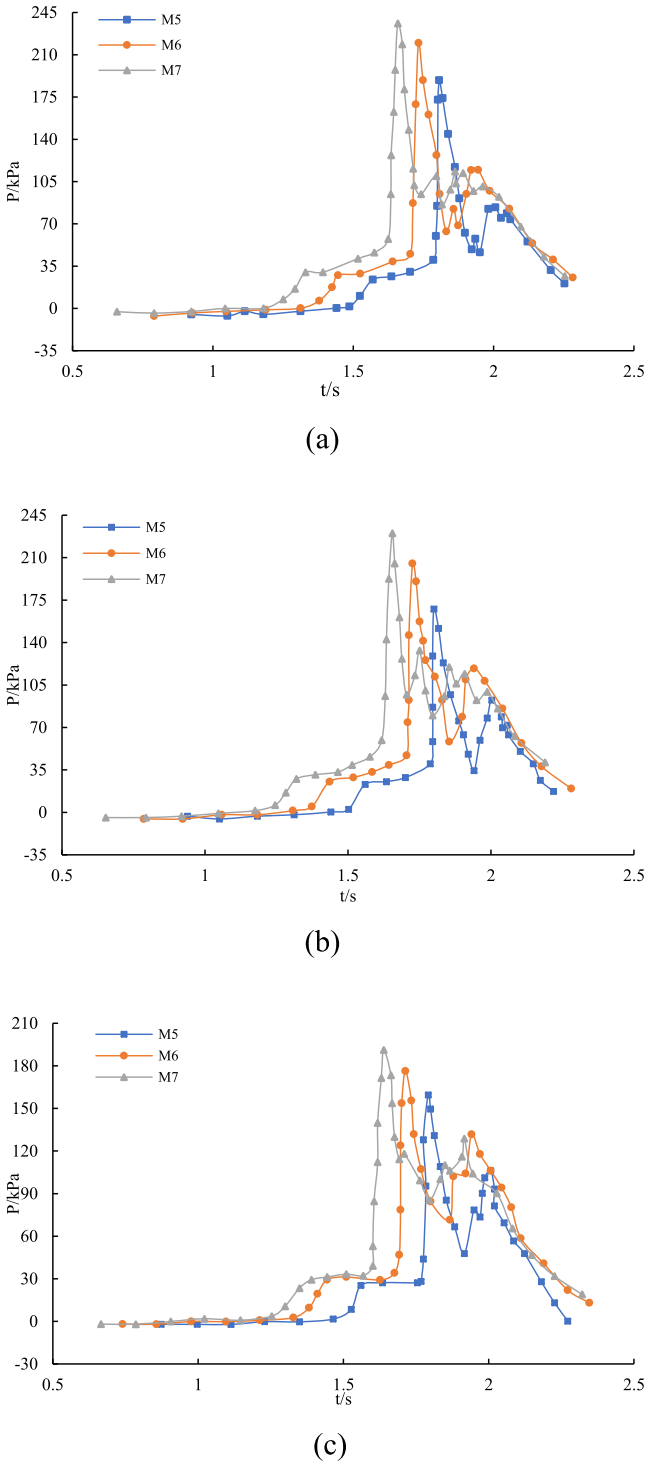

Figure 17. Overpressure curves of the roadway under three explosion venting pressures. (a) Explosion pressure of 200 kPa. (b) Explosion pressure of 150 kPa. (c) Explosion pressure of 50 kPa.

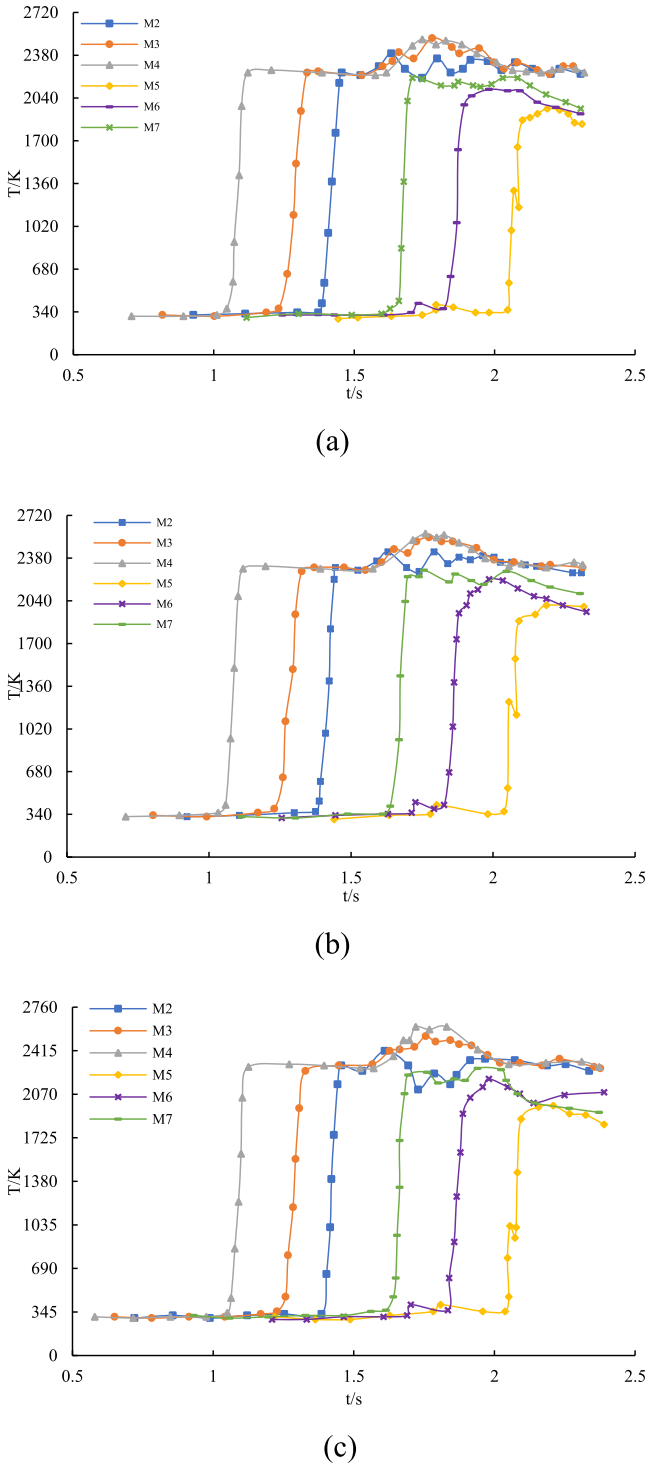

Figure 18. Temperature curves of the roadway under three explosion venting pressures. (a) Explosion pressure of 200 kPa. (b) Explosion pressure of 100 kPa. (c) Explosion pressure of 50 kPa.

the first corresponding to the scenario when the net pressure acts in the negative direction and the second corresponding to the scenario when the net pressure acts in the positive direction. For example, if the given pressure values are −100 and 200 kPa, the blast wall begins to yield when the net pressure is less than −100 kPa (negative direction) or greater than 200 kPa (positive direction). In this simulation, the venting pressures of the venting wall were set to 200, 100, and 50 kPa.

The area porosity (φ) of the blast wall ranged from 0 (fully closed state) to 1 (fully open state). In the setting of the explosion vent wall weight (m), the unit of weight is in kg/m2, that is, mass per unit area. If the weight is set to zero, the inertial force can be ignored during the dynamic process when the blast wall yields under pressure during the simulation. In this simulation, the weight of the blast wall was set to 50 kg/m2. Parameters such as resistance coefficient and maximum

https://doi.org/10.1021/acsomega.2c05740
ACS Omega 2023, 8, 5257−5273

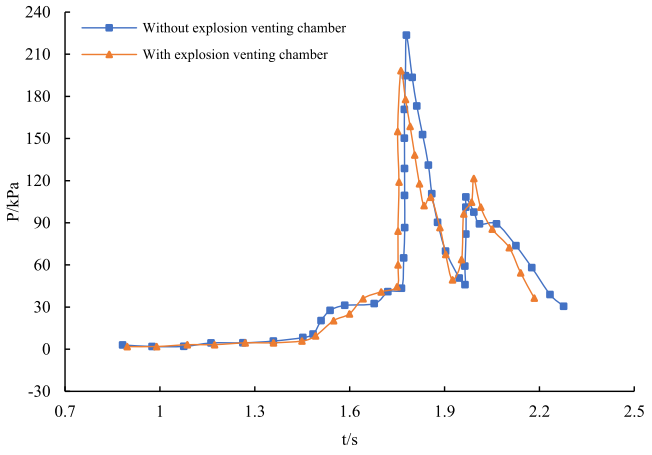

(a)

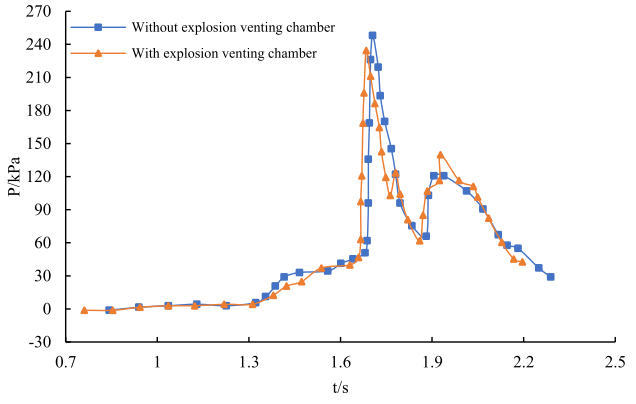

(b)

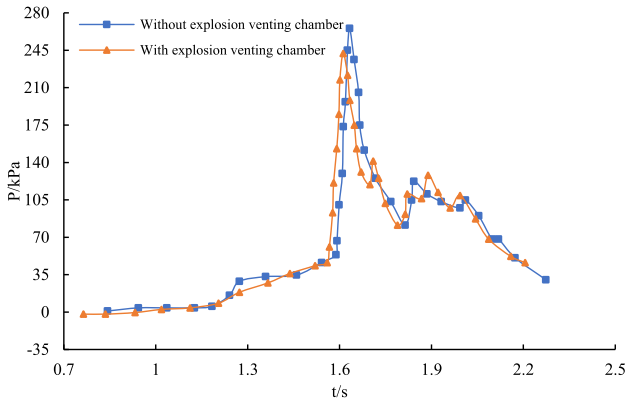

(c)

Figure 19. Comparison of overpressure in the roadway with or without the explosion venting chamber. (a) Overpressure of monitoring point M5. (b) Overpressure of monitoring point M6. (c) Overpressure of monitoring point M7.

displacement length are automatically provided by the software and need not be set manually.

4.3. Variation Trend of Overpressure under Three Explosion Venting Pressures. Figures 16 and 17, respectively, describe the variation law of the overpressure values of M2, M3, and M4 in the excavation roadway and M5, M6, and M7 in the main roadway with the explosion time

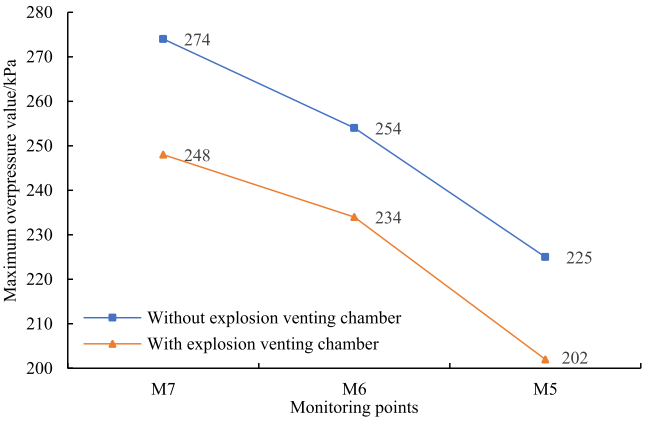

Figure 20. Comparison of maximum overpressure in the roadway with or without the explosion venting chamber.

under the three explosion relief pressures. Combined with the analysis of the images, we can observe that the propagation law of the shock wave from the formation to the breaking of the explosion venting wall into the venting chamber was generally similar to that of the scenario without the venting wall; therefore, the trend of the overpressure curve was also similar. After gas explosion, although the explosion pressure differed, the overpressure variation trend of each measuring point in the roadway was the same. The closer to the explosion source point, the shorter the time of overpressure reaching the peak value, and the farther away from the explosion source point, the longer the time of overpressure reaching the peak value.

During shock wave propagation, the shock wave oscillated owing to the reflections at the wall, the reflection at the head, the explosion vent wall, and the reflection at the bend of the roadway. After the blast wall yielded, the shock wave entered the blast chamber, and a positive reflection occurred. Most of the reflected shock waves reached the tunnel, resulting in more oscillations in the overpressure curves of measuring points M2−M4.

As the reaction advanced, the explosion overpressure curve eventually stabilized after several fluctuations, which indicated that the explosion overpressure was not monotonically increasing or decreasing over time but fluctuating. When the explosion reaction was complete, the energy of the shock wave was gradually consumed owing to multiple reflections. After a period of propagation, the precursor wave no longer compressed the gas ahead and finally propagated at a stable speed. Here, the overpressure of each measuring point tended to be stable and did not change.

4.4. Variation Trend of Temperature under Three Explosion Venting Pressures. Figure 18 describes the variation in the temperature values of M2, M3, and M4 in the excavation and M5, M6, and M7 in the roadway with explosion time under three explosion venting pressures. The changing law of the curve was the same as that of the scenarios with and without an explosion venting chamber.

We observed that although the explosion pressure differed, the flame temperature variation of each measuring point was the same, which increased gradually initially and then abruptly increased and finally stabilized. The closer to the explosion source point, the shorter the time for the temperature to reach the peak and the higher the temperature.

Before the flame front reached each measuring point, as the gas was ignited, the flame began to spread gradually, and the

https://doi.org/10.1021/acsomega.2c05740
ACS Omega 2023, 8, 5257−5273

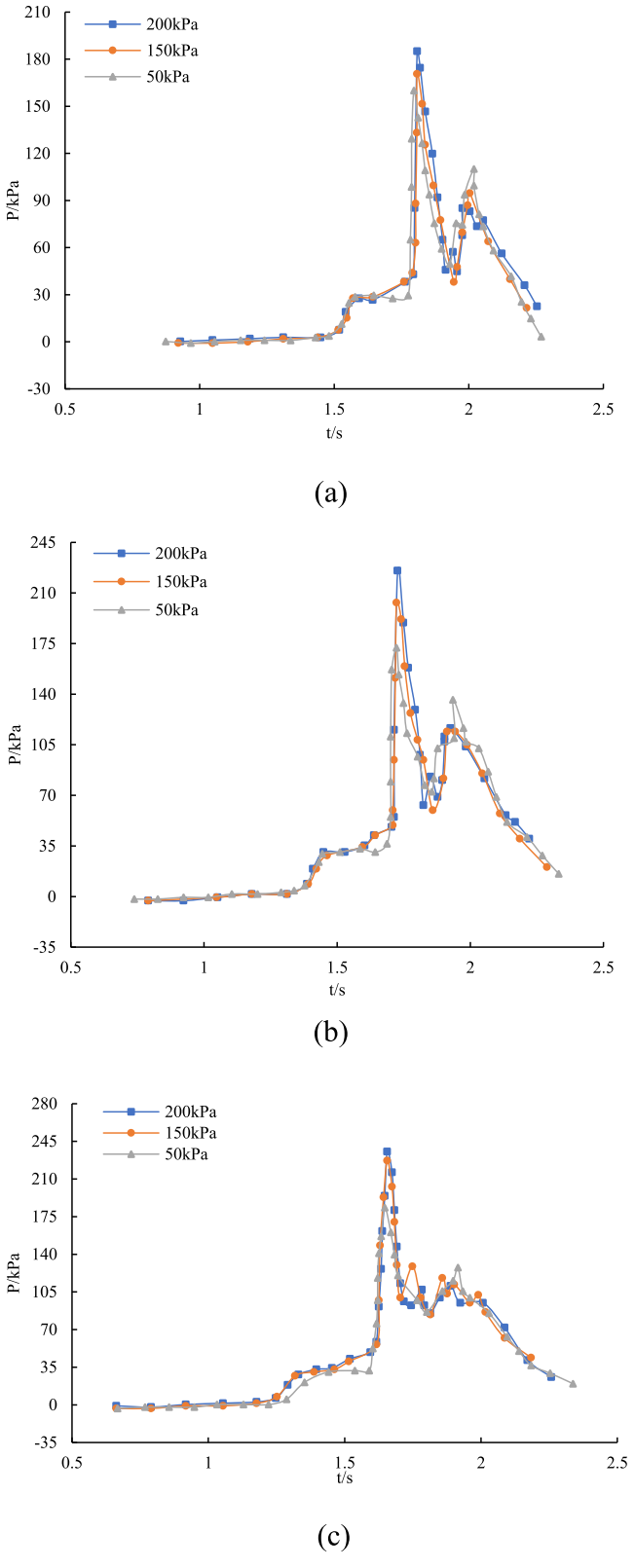

Figure 21. Comparison of overpressure in the roadway under different explosion venting pressures. (a) Overpressure of monitoring point M5. (b) Overpressure of monitoring point M6. (c) Overpressure of monitoring point M7.

temperature of each measuring point increased gradually. When the flame front reached and passed through each measuring point, a large amount of combustion heat was released, and the temperature of each measuring point increased abruptly. In addition, the temperature curve fluctuated after the sudden increase in temperature, which was because the flame wave entered the turning part, the combustion was uneven, the flame was close to the exit, and the heat spread out rapidly from the exit, coupled with the backflow of the outlet airflow, resulting in temperature fluctuations.

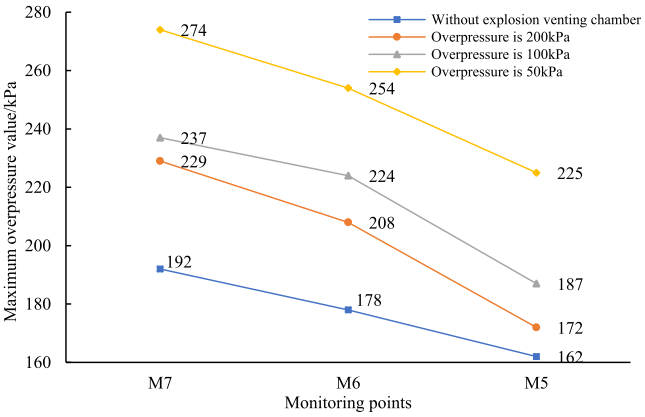

Figure 22. Comparison of maximum overpressure in the roadway under different explosion venting pressures.

5. RESULTS AND DISCUSSION

5.1. Comparative Analysis of Overpressure. As the shock wave overpressure is the main parameter to describe the properties of shock waves, studying it is vital. The shock wave overpressure is related to the shock wave energy and distance from the explosion center. The overpressure criterion states that the explosion overpressure only determines whether the shock wave will cause damage. To cause damage to the target, the shock wave overpressure must exceed a certain value; otherwise, the shock wave will not cause damage to the target. Therefore, the explosion overpressure of each measuring point in the roadway after the gas explosion was compared and analyzed under different conditions.

5.1.1. Comparative Analysis of Overpressure with and without the Explosion Venting Chamber. Figure 19 shows that the maximum overpressure of each measuring point was less with the explosion chamber than without the explosion chamber. In the scenario with an explosion venting chamber, the existence of the explosion venting chamber increased the number of reflections of the shock wave; therefore, the overpressure curve of each measuring point had more peaks and oscillations.

The overpressure curve of measuring point M7 in the abovementioned figure shows that near the corner of the roadway and explosion chamber, the number of reflections of the shock wave was more, and the overpressure oscillation curve was more intense. Therefore, the closer to the corner of the roadway and explosion chamber, the stronger the oscillation of the overpressure curve was.

Figure 20 can clearly show that the closer the monitoring point was to the roadway bend and explosion venting chamber, the greater the maximum overpressure value. With the explosion chamber, the maximum overpressure of each measuring point in the large roadway was lower than that without an explosion chamber. The existence of the explosion chamber reduced the overpressure of measuring points M5,

https://doi.org/10.1021/acsomega.2c05740
ACS Omega 2023, 8, 5257−5273

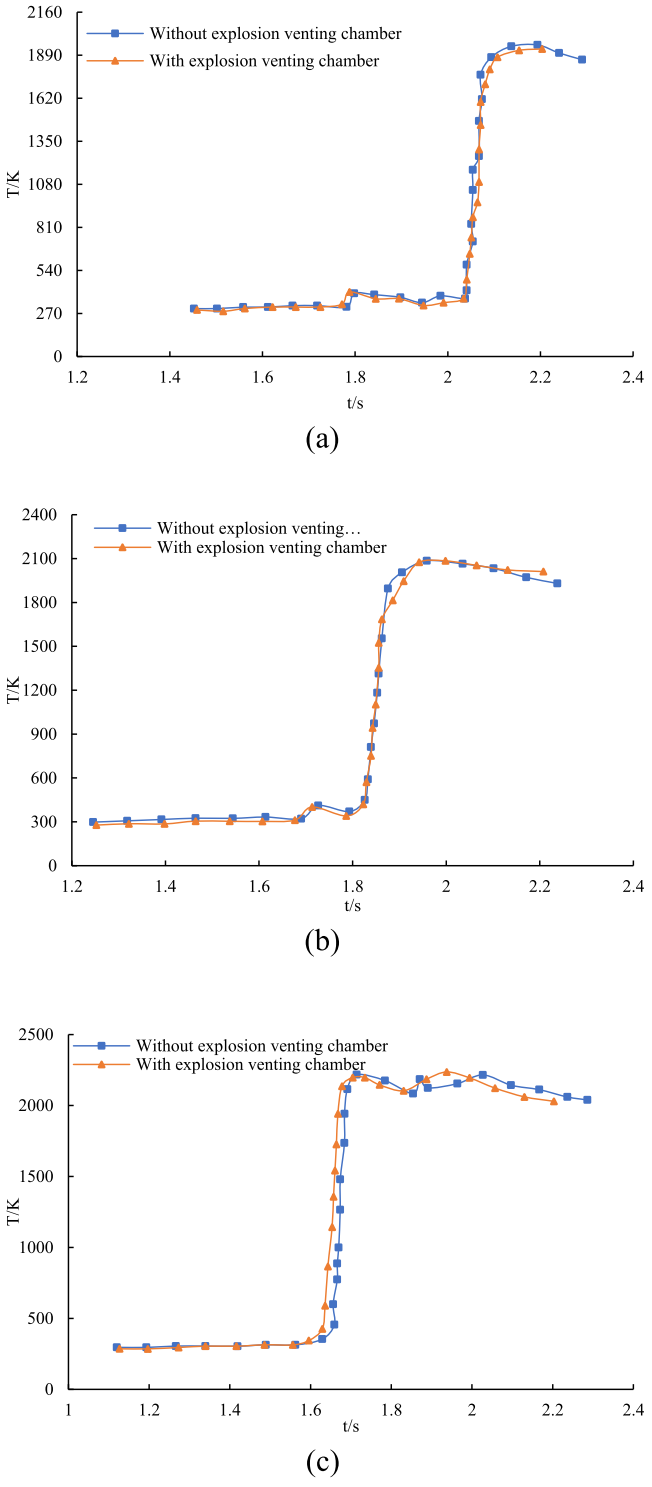

Figure 23. Comparison of temperature in the roadway under different explosion venting pressures. (a) Temperature of monitoring point M5. (b) Temperature of monitoring point M6. (c) Temperature of monitoring point M7.

M6, and M7 by 23, 20, and 26 kPa, respectively. Compared with the case without the explosion chamber, the overpressure value decreased by about 10.2, 7.9, and 9.5%, respectively.

We can conclude that after the shock wave generated by the gas explosion entered the explosion venting chamber, the shock wave was repeatedly reflected, which reduced the shock wave overpressure on both sides of the road to a certain extent.

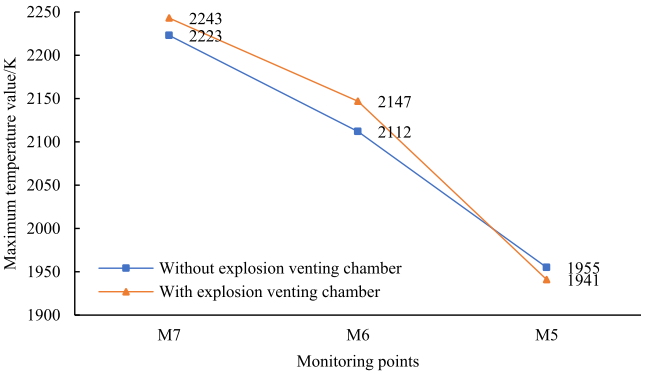

Figure 24. Comparison of maximum temperature in the roadway with or without the explosion venting chamber.

The effect of pressure relief was not apparent, and the reduction in the overpressure is about 10%.

5.1.2. Comparative Analysis of Overpressure with the Explosion Vent Wall. Figure 21 describes the overpressure curves of each measuring point in the roadway under three different explosion pressures. We observed that the maximum overpressure of each measuring point decreased with the decrease in the explosion pressure.

The overpressure curve of monitoring point M7 in Figure 21 shows that the closer to the turn of the roadway, blast wall, and blast chamber, the more times the shock wave was reflected; thus, the overpressure curve oscillated more strongly. The time that each measuring point reached the maximum overpressure under different venting pressures was the same.

Figure 22 clearly shows that the overpressure at each measuring point in the main roadway decreased with the decrease in the explosion venting pressure. When the blast pressure of the blast wall was 200 kPa, the overpressures of monitoring points M5, M6, and M7 decreased by 23, 30, and 37 kPa, respectively. Compared with the scenario with no venting chamber and no venting wall, the overpressure value decreased by about 16.9, 11.8, and 13.5%, respectively.

When the blast pressure of the blast wall was 100 kPa, the overpressures of M5, M6, and M7 decreased by 53, 46, and 82 kPa, respectively. Compared with the scenario with no venting chamber and no venting wall, the overpressure value has decreased by about 23.6, 18.1, and 16.4% respectively.

When the blast pressure of the blast wall was 50 kPa, the overpressure of M5, M6, and M7 decreased by 63, 76, and 82 kPa, respectively. Compared with the scenario with no venting chamber and no venting wall, the overpressure value decreased by about 28.0, 29.9, and 30.0%, respectively.

We can conclude that the overpressure in the main road decreased by about 15% when the explosion pressure was 200 kPa; when the explosion pressure was 100 kPa, it decreased by about 20%; when the explosion pressure was 50 kPa, it decreased by about 30%, that is, when the venting pressure of the venting wall was 50 kPa, the venting effect was the best.

5.2. Comparative Analysis of Temperature. A flame is generated after a gas explosion, and the damage it causes is a special type of composite damage. It can not only burn the target but also produce shock waves and toxic and harmful gases, which often occur in coal mining and tunneling working faces. Therefore, the flame temperature of each measuring point in the alley after the gas explosion under different conditions was compared and analyzed.

https://doi.org/10.1021/acsomega.2c05740
ACS Omega 2023, 8, 5257−5273

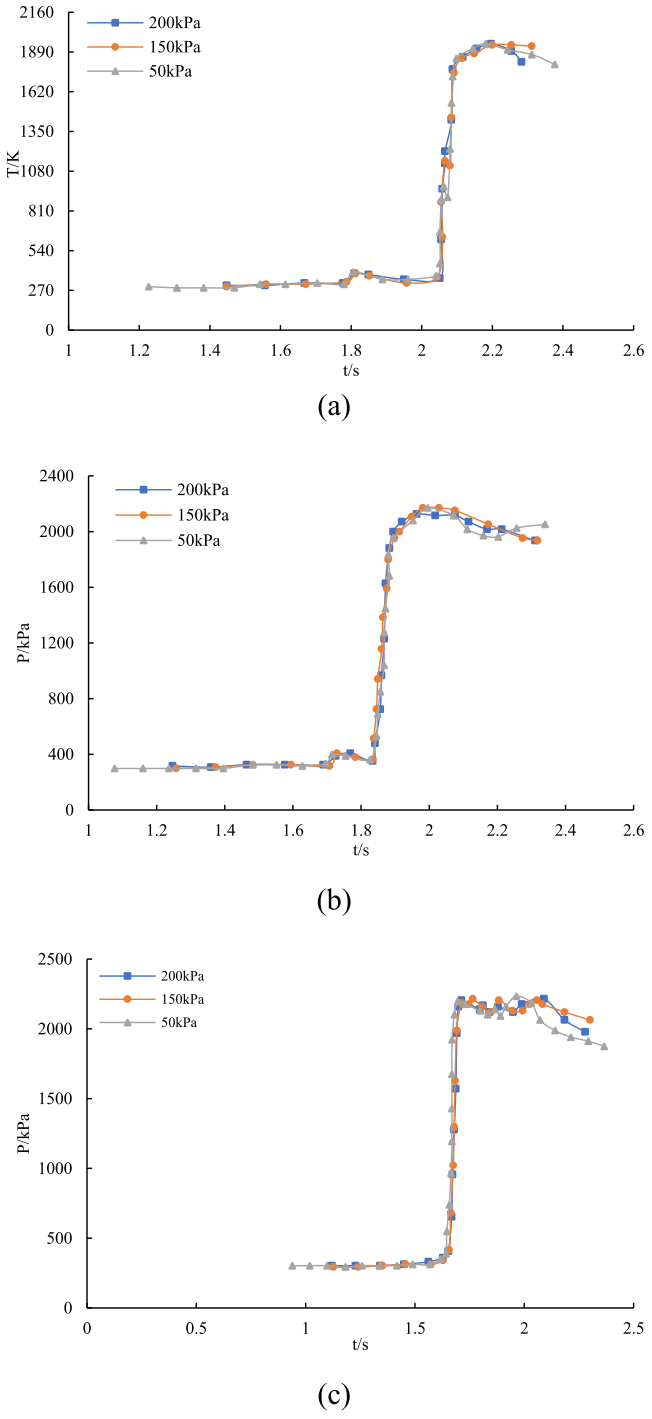

Figure 25. Comparison of temperature in the roadway under different explosion venting pressures. (a) Temperature of monitoring point M5. (b) Temperature of monitoring point M6. (c) Temperature of monitoring point M7.

5.2.1. Comparative Analysis of Temperature with and without the Explosion Venting Chamber. Figure 23 shows that the temperature of each measuring point in the alley had basically the same trend of change in the presence or absence of the explosion venting chamber, and the temperature initially increased gradually. When the flame reached the measuring point, the temperature increased abruptly. The temperature reached a maximum value and then exhibited a fluctuating state and tended to stabilize owing to uneven combustion at the outlet and gas recirculation.

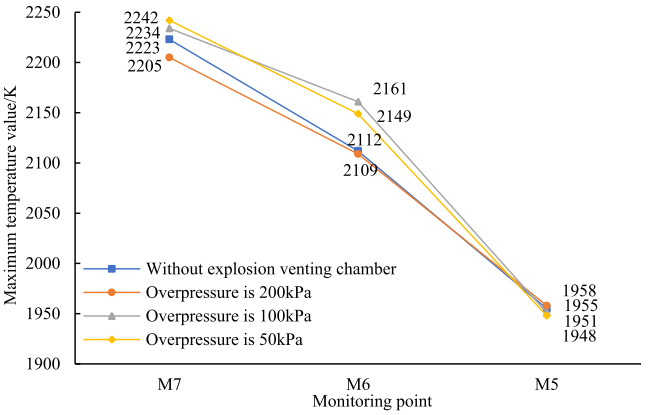

Figure 26. Comparison of maximum temperatures in the roadway under different explosion venting pressures.

Figure 24 clearly shows the maximum temperature value of each measuring point in the roadway in the two scenarios with or without the explosion venting chamber. The maximum temperature of each measuring point with the explosion chamber was slightly higher than that without the explosion chamber, but the temperature difference was not significant. The maximum temperature differences of measuring points M7, M6, and M5 were 20, 35, and 14 K, respectively.

We can conclude that the explosion venting chamber has a slight effect on the temperature of each measuring point in the roadway after the gas explosion.

5.2.2. Comparative Analysis of Temperature with the Explosion Vent Wall. Figure 25 shows that the temperature of each measuring point in the alley was basically the same under different explosion venting pressures, and they all increased gradually initially. When the flame reached the measuring point, the temperature abruptly increased to the maximum value. Because of the non-uniform combustion at the outlet and the gas backflow, it exhibited a fluctuating state and tended to be stable.

Figure 26 shows that the maximum temperature value of each measuring point in the roadway differed under different explosion venting pressures, but the temperature difference was not large. The maximum temperature difference of M5 was 7 K; the maximum temperature difference of M6 was 52 K; and the maximum temperature difference of M7 was 37 K.

We can conclude that the blast wall with different blast pressures has a slight effect on the temperature of each measuring point in the roadway after the gas explosion.

5.3. Comparative Analysis of Explosive Impulse. The overpressure criterion ignores the time factor of the overpressure acting on the target. If the overpressure value is the same and if the duration of the action on the target is different, then the destructive effect on the target is also different. Based on this defect of the overpressure criterion, experts and scholars have proposed the impulse criterion through theoretical analysis and a large number of experiments: When the impulse I (Pa·s) of the shock wave reaches a certain value, it will cause a corresponding degree of damage to the target. It can be clearly seen from the unit of impulse that the impulse criterion takes into account the time of overpressure. However, the impulse criterion also has its shortcomings. It ignores that if the overpressure is too small,

https://doi.org/10.1021/acsomega.2c05740
ACS Omega 2023, 8, 5257−5273

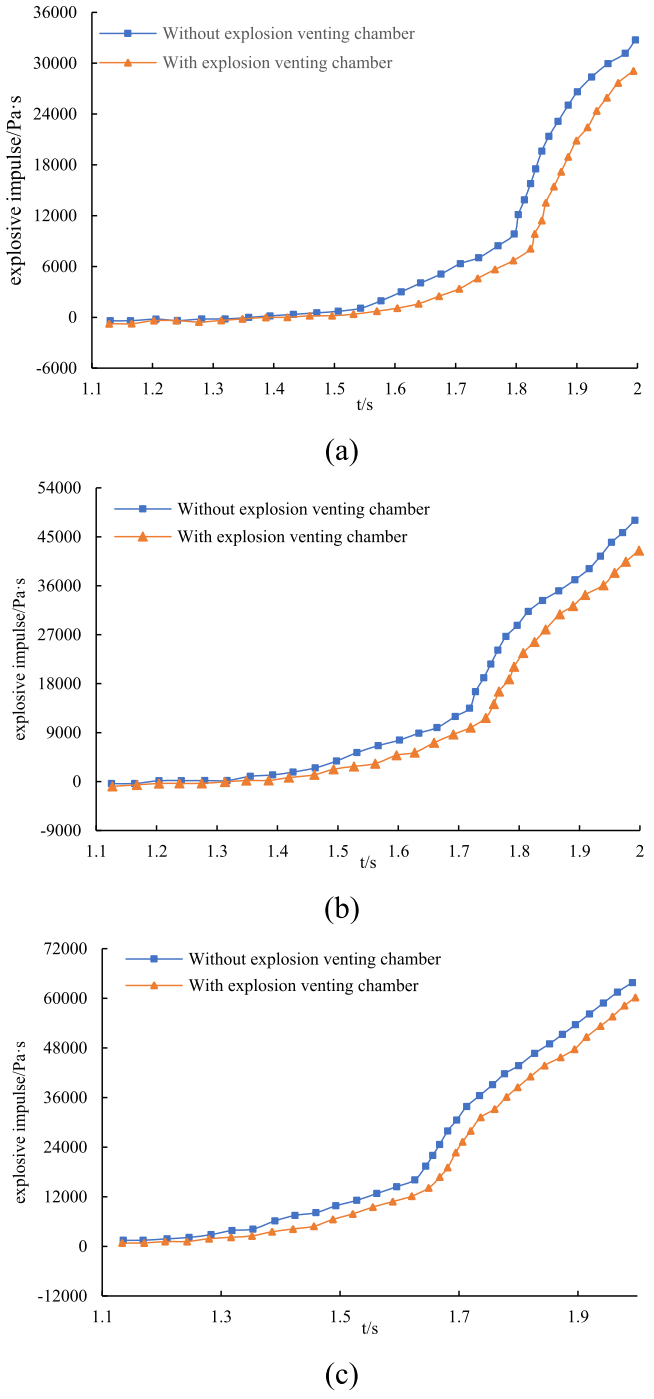

Figure 27. Comparison of explosive impulse in the roadway with or without the explosion venting chamber. (a) Explosive impulse of monitoring point M5. (b) Explosive impulse of monitoring point M6. (c) Explosive impulse of monitoring point M7.

how long the action time is, and the target will not be destroyed.

5.3.1. Comparative Analysis of Explosive Impulse with and without the Explosion Venting Chamber. The explosion impulses of each measuring point in the roadway within 2s after gas explosion were compared and analyzed in two cases with or without the explosion venting chamber. Figure 27 shows that at the beginning of the explosion, the impulse curve also increases slowly because of the slow increase in pressure. When the explosion pressure increases suddenly, the impulse also increases greatly and the impulse curve steepens. In both cases, the change trend of the impulse time curve is consistent, but the curve with the explosion venting chamber is gentler than that without the explosion venting chamber, and the explosion impulse value is relatively small at the same time, indicating that the explosion venting chamber can reduce a part of the shock wave damage effect.

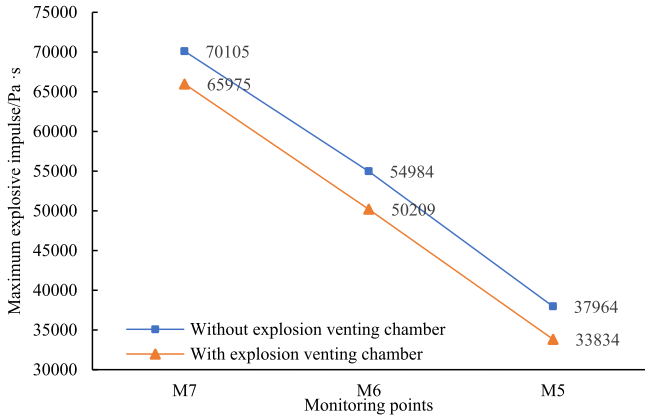

Figure 28. Comparison of the maximum explosive impulse with or without the explosion venting chamber.

Figure 28 can clearly show that in the case of the explosion venting chamber, the maximum explosion impulse of each measuring point in the large roadway is lower than that without the explosion venting chamber, and the closer the measuring point is to the corner of the roadway and the explosion venting chamber, the greater the explosion impulse. The explosion impulse of M5, M6, and M7 measuring points decreased by 4130, 4775, and 4130 Pa·s, respectively, due to the existence of the explosion venting chamber. Compared with the situation without the explosion venting chamber, the overpressure value decreased by about 5.9, 8.7, and 10.9%, respectively.

We can conclude that the explosion venting chamber can reduce the shock wave impulse on both sides of the roadway, and the explosion impulse is reduced by about 8.5%.

5.3.2. Comparative Analysis of the Explosive Impulse with the Explosion Vent Wall. The following figure (Figure 29) makes a comparative analysis of the explosion impulse at each measuring point in the roadway within 2s after the gas explosion under the conditions of three kinds of detonation pressure. Figure 29 shows that at the beginning of the explosion, the impulse curve also increases slowly due to the slow increase in pressure. When the explosion pressure increases suddenly, the impulse also increases greatly and the impulse curve steepens. In the case of different venting pressures, the change trend of the impulse time curve is consistent, but with the decrease in venting pressure, the value is also relatively small. The change trend of the curve with time is more and more gentle, and at the same time, the smaller the discharge pressure is, the smaller the explosion impulse value is.

Figure 30 clearly shows that the maximum explosion impulse of each measuring point in the large tunnel decreases with the decrease in explosion pressure. When the venting pressure of the venting wall is 200 kPa, the maximum explosion impulses of M5, M6, and M7 measuring points are reduced by 5464, 6546, and 7982 Pa·s, respectively. Compared with the case without the venting chamber and venting wall, the maximum

https://doi.org/10.1021/acsomega.2c05740
ACS Omega 2023, 8, 5257−5273

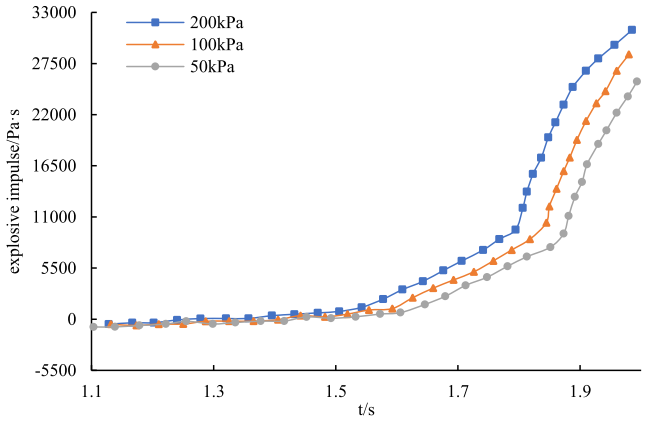

(a)

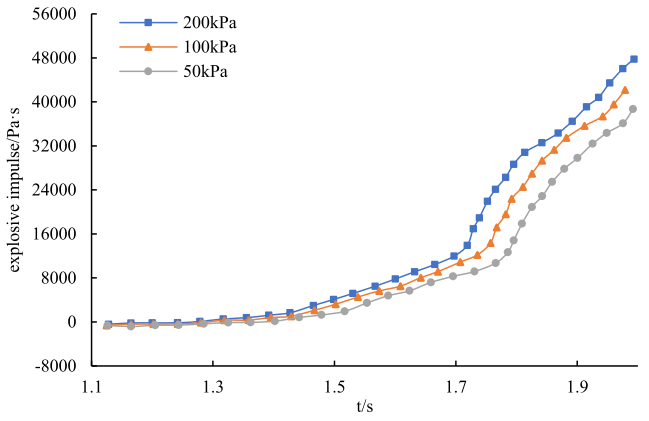

(b)

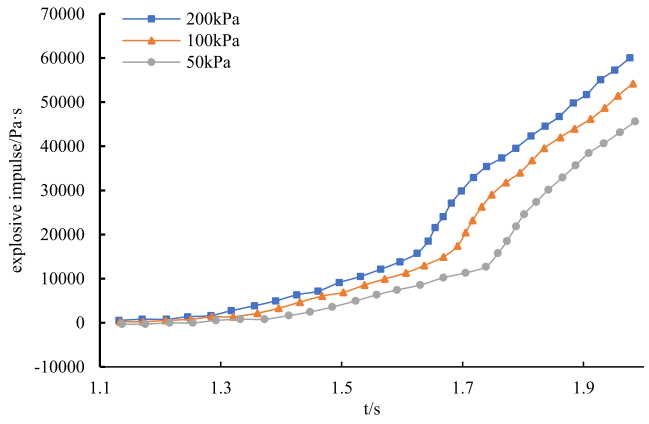

(c)

Figure 29. Comparison of explosive impulse in the roadway under different explosion venting pressures. (a) Explosive impulse of monitoring point M5. (b) Explosive impulse of monitoring point M6. (c) Explosive impulse of monitoring point M7.

explosion impulse value decreased by about 14.4, 12.0, and 11.4%, respectively.

When the venting pressure of the venting wall is 100 kPa, the maximum explosion impulses of M5, M6, and M7 measuring points are reduced by 8271, 11051, and 13318 Pa·s, respectively. Compared with the case without the venting chamber and venting wall, the maximum explosion impulse value decreased by about 21.8, 20.1 and 19.0%, respectively.

When the venting pressure of the venting wall is 50 kPa, the maximum explosion impulses of M5, M6, and M7 measuring points are reduced by 11630, 15786, and 22598 Pa·s, respectively. Compared with the case without the venting chamber and venting wall, the maximum explosion impulse value decreased by about 30.6, 28.7 and 32.3%, respectively.

We can conclude that the maximum explosion impulse in the roadway is reduced by about 13% when the explosion pressure is 200 kPa. When the explosion pressure is 100 kPa, it is reduced by about 20%; when the venting pressure is 50 kPa, it is reduced by about 31%, that is, when the venting pressure of the venting wall is 50 kPa, the venting effect is the best.

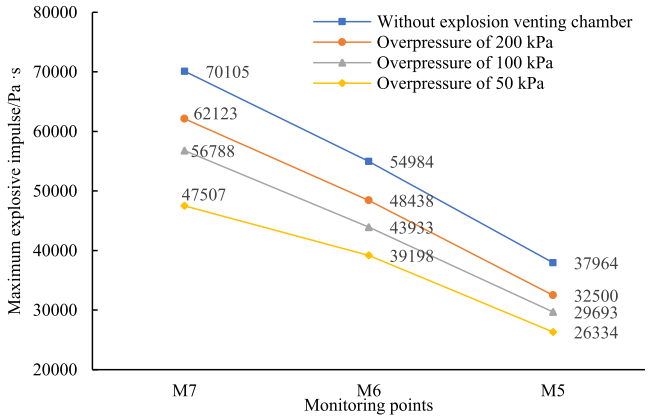

Figure 30. Comparison of the maximum explosive impulse in the roadway under different explosion venting pressures.

6. CONCLUSIONS

In this paper, the models of the excavation roadway, the forward venting chamber, and the venting wall are established. When the gas explosion occurs in the heading face, the overpressure propagation law and flame temperature law of the heading roadway and the main roadway under the action of the forward chamber and the blasting wall are simulated. The overpressure, temperature, and explosive impulse of each measuring point in the main road are analyzed and compared, and the effect of explosion venting under different explosion venting conditions is analyzed based on this.

(1) The existence of the venting chamber reduces the overpressure of each measuring point in the alley by 10%, and explosive impulse reduced by 8.5%, indicating that the venting chamber has a certain venting effect.

(2) The explosion venting wall can effectively reduce the overpressure and explosive impulse in the roadway. When the pressure of the venting wall is 200, 100, and 50 kPa, the overpressure in the roadway is reduced by 15, 20, and 30%, respectively. The maximum explosion impulse is reduced by 13, 20, and 31%, respectively.

(3) As the venting pressure of the venting wall decreases, the venting effect becomes increasingly better. When the venting pressure of the venting wall is 50 kPa, the venting effect is the best.

https://doi.org/10.1021/acsomega.2c05740
ACS Omega 2023, 8, 5257−5273

AUTHOR INFORMATION

Corresponding Author

Ke Gao − *College of Safety Science and Engineering, Liaoning Technical University, Huludao 125000, China; Key Laboratory of Mine Thermodynamic Disasters and Control of Ministry of Education, Liaoning Technical University, Huludao 125000, China*; Email: gaoke@lntu.edu.cn

Authors

Zemiao Yang − *College of Safety Science and Engineering, Liaoning Technical University, Huludao 125000, China; Key Laboratory of Mine Thermodynamic Disasters and Control of Ministry of Education, Liaoning Technical University, Huludao 125000, China*; orcid.org/0000-0002-3302-6122

Shuai Yang − *College of Safety Science and Engineering, Liaoning Technical University, Huludao 125000, China; Key Laboratory of Mine Thermodynamic Disasters and Control of Ministry of Education, Liaoning Technical University, Huludao 125000, China*

Shengnan Li − *College of Safety Science and Engineering, Liaoning Technical University, Huludao 125000, China; Department of Mechanical Engineering, National University of Singapore, Singapore 117576, Republic of Singapore*; orcid.org/0000-0002-9046-388X

Complete contact information is available at: https://pubs.acs.org/10.1021/acsomega.2c05740

Notes

The authors declare no competing financial interest.

ACKNOWLEDGMENTS

This work was financially supported by the Natural Science Foundation of China (nos. 52074148 and 52104194) and the Foundation of Liaoning Educational Committee (no. LJKZ0341).

REFERENCES

(1) Wang, X. Analysis on the status quo and countermeasures of green mining of coal resources. *J. Technology Wind.* **2021**, *36*, 154−156.

(2) Duan, W. Current situation and sustainable development of coal resources utilization. *J. Mining Equipment.* **2022**, *02*, 134−135.

(3) Yang, F. Analysis on Demand Prospect of Coal Products in Electric Power Industry of China. *J. China Coal.* **2020**, *46*, 22−31.

(4) *Coal mine safety net*. Accident Express[EB/OL]. 2020(2020-12-28) [2021-01-09].

(5) *Coal Mine Safety Supervision Office*. Safety Alert [EB/PL]. 2020, (2020-09-06) [2021-01-09].

(6) Zhang, P.; Lee, F.; Zhu, H.; Niu, H.; Lee, X. Statistical Analysis and Countermeasures of Coal Mine Accidents from 2008 to 2020. *J. Mining Safety Environmental Protection* **2022**, *49*, 128−134.

(7) Cao, W.; Shi, J.-Q.; Durucan, S.; Si, G.; Korre, A. Gas-driven rapid fracture propagation under unloading conditions in coal and gas outbursts. *J. International Journal of Rock Mechanics and Mining.* **2020**, *130*, 104325.

(8) Wang, X. *Research on ventilation system of metal mine at high altitude*; D. University of Science and Technology Beijing, 2015.

(9) Xin, S. *Plateau mine ventilation*; M. BeijingChina Coal Industry Press, 2015.

(10) Zhu, Y.; Wang, D.; Shao, Z.; Xu, C.; Zhu, X.; Qi, X.; Liu, F. A statistical analysis of coalmine fires and explosions in China. *Process Saf. Environ. Prot.* **2019**, *121*, 357−366.

(11) Yu, M.; Yang, X.; Zheng, K.; Luan, P. Progress and development of coal mine gas explosion suppression and disaster reduction technology in China. *J. China Coal Soc.* **2020**, *45*, 168−188.

(12) Liu, X.; Liu, J.; Qu, M. Numerical simulation on flame propagation laws of gas explosion in excavation roadway of high-altitude mines. *J. Journal of Safety Science and Technology* **2020**, *16*, 67−71.

(13) Gregroy, P. S.; David, M. G.; Michael, F.. Gri-Mech 3.0 [EB/OL] (2019-12-05) [2020-12-2]. http://www.me.berkeley.edu/gri_mech/.

(14) Luo, Z.; Kang, X.; Wang, T.; Su, B.; Jia, Y. Numerical simulation of explosion process of different gas sources in driving face. *J. Coal Mine Safety.* **2020**, *51*, 166−170.

(15) Han, R.; Liu, J.; Gao, K.; Lai, X. Research on the influence of obstacles in a confined space on the propagation of gas explosion. *J. Journal of Safety Science and Technology* **2018**, *14*, 61−66.

(16) Ke, G.; Li, S.-N.; Han, R.; Li, R.-Z.; Liu, Z.-M.; Qi, Z.-P.; Liu, Z.-Y. Study On the propagation law of gas explosion in the space based on the goaf characteristic of coal mine. *J. Safety Science.* **2020**, *127*, 104693.

(17) Li, R.; Si, R.; Gao, K.; Qin, X.; Wen, L. Experimental study on the effect of explosion suppression in low-concentration gas transportation. *J. Loss Prev. Process Ind.* **2018**, *54*, 216−221.

(18) Bai, G.; Zhou, X.; Song, D. Experiment on the effect of temperature and CO gas coupling on gas explosion limit. *J. Pressure Physics.* **2019**, *33*, 189−196.

(19) Dorofeev, S. B. Flame acceleration and explosion safety applications. *J. Proceedings of the Combustion Institute.* **2011**, *33*, 2161−2175.

(20) Lee, J. H. S.; Solohukhin, R. I.; Oppenheim, A. K. Current views on gaseous detonation. *J. Astonautica Acta.* **1969**, 565−584.

(21) Ciccarelli, G.; Dorofeev, S. Flame acceleration and transition to detonation in ducts. *J. Progress in Energy and Combustion Science* **2008**, *34*, 499−550.

(22) Oran, E. S.; Vadim, N. Origins of the deflagration-to-detonation transition in gas-phase combustion. *J. Combustion ang Flame.* **2007**, *148*, 4−47.

(23) Baoshan, J.; Yanhong, L.; Wen, Z. Sensitivity analysis of gas explosion chain reaction mechanism in confined space. *J. Environmental Engineering.* **2011**, *29*, 318−323.

(24) Berthelot, M.; Meille, E. On the velocity of propagation of explosive processes in gases. *J. C. R. Hebd. Sciences Acad. Sci* **1881**, *93*, 18−21.

(25) Kangan, L. On the Transion from Deflagration to Detonation in Narrow Channeis. *J. Math. Model. Nat. Phenom.* **2003**, *2*, 389−397.

(26) Fairweather, M.; Ibrahim, S. S.; Jaggers, H.; Walker, D. G. Turbulent premixed flame propagation in a cylindrical vessel. *C. Symposium (International)on Combustion Elsevier* **1996**, *26*, 365−371.

(27) Fairweather, M.; Hargrave, G. K.; Ibrahim, S. S.; Walker, D. G. Studies of premixed flame propagation in explosion tubes. *J. Combustion and Flame.* **1999**, *116*, 504−518.

(28) Lebecki, K. Gasdynamic. Phenomena Occurring in Coal Dust Explosion. *J. Przegl Gom.* **1980**, *36*, 243−247.

(29) Sa Wenke, C. K. *Underground air shock wave*; M. BeijingMetallurgical Industry Press, 1979.

(30) Tao, L.; Jinzhang, J. Overpressure Prediction of Gas Explosion Shock Wave in Coal Mine Roadway. *J. Mining Safety Environmental Protection.* **2017**, *44*, 18−20.

(31) Wagner, H. G. *A. in 'Fuel Air Explosion'*; University of waterloo Press, 1982, pp 77−79.Some experiments about flame acceleration

(32) Moen, I. O. The influence of turbulence on flame propagation in obstacle environments. In *Fuel Air Explosion*; University of waterloo Press, 1982, pp 138−140.

(33) Alexiou, A.; Andrews, G. E.; Phylaktou, H. Side-vented gas explosions in a long vessel: the effect of vent position. *J. Journal of Loss Prevention in the Process Industries.* **1996**, *9*, 351−356.

(34) Liebman, I. Passive explosion barrier for mines. U.S.Patent 4,284,144 A, 1981.

https://doi.org/10.1021/acsomega.2c05740
ACS Omega 2023, 8, 5257−5273

(35) Hertzberg, M. *Inhibition and extinction of coal dust and methane explosions*; M. US Department of the Interior, Bureau of Mines, 1982.
(36) Cheng, L.; Richard Pro, M. *Bureau of mines report of investigations*, 1984. (RI 8915).
(37) Cortese, R. A.; Sapko, M. J. *Flame-powered trigger device for activating explosion suppression barrier*; M. Bureau of Mines (RI 9375), 1991.
(38) Lebecki, K.; Cybulski, K.; Dyduch, Z.; Wolański, P. Large Scale Grain Dust Explosions-Research in Poland. *J. Shock Waves* **1995**, 109−114.
(39) Xia, Z.; Cai, Z. *YBW-I Model of Trigger Explosion Suppressor*; R. Report of Chongqing Branch of Chongqing Branch of Central Coal Research Institute: Chongqing, 1998.
(40) Klemens, R.; Szatan, B.; Gieras, M.; Piotr, W.; Maranda, A.; Jerzy, N.; Józef, P. Suppression of dust explosions by means of different explosive charges. *J. Journal of Loss Prevention in the Process Industries* **2000**, *13*, 265−275.
(41) Krasnyansky, M. Prevention and suppression of explosions in gas-air and dust-air mixtures using powder aerosol-inhibitor. *J. Journal of Loss Prevention in the Process Industries* **2006**, *19*, 729−735.
(42) Oleszczak, P.; Klemens, R. Mathematical modelling of dust-air mixture explosion suppression. *J. Journal of Loss Prvention in the Process Industries.* **2006**, *19*, 187−193.
(43) Mingwei, Y.; Weibin, F.; Juncheng, J. Experimental study on gas-tight explosion and venting process of connected container. *J. Journal of Safety Science and Technology* **2014**, *10*, 11−15.
(44) Wei, S.; Zhirong, W.; longsheng, M.; Minghan, L.; Chenjian, Y. Influencing factors of explosion venting process of connected container. *J. Explosion and Shock Waves* **2016**, *36*, 457−464.

https://doi.org/10.1021/acsomega.2c05740
ACS Omega 2023, 8, 5257−5273